*Journal of Fluids and Structures* (1997) **11,** 947–963

# LIQUID SLUG MOTION IN A VOIDED LINE

Z. Bozkus* and D. C. Wiggert

*Department of Civil and Environmental Engineering, Michigan State University East Lansing, MI 48824, U.S.A.*

(Received 12 June 1996 and in revised form 17 June 1997)

Transient individual liquid slug motion in a voided line is investigated both numerically and experimentally. In a series of experiments, slugs of various lengths are propelled into an empty pipe under varying air pressures controlled at an upstream reservoir. The pressure–time histories created by the impacting slugs at an elbow located at the end of the pipe reach are measured, and the peak pressures are in reasonable agreement with results reported in an earlier study. An analytical model is developed to predict the slug acceleration and its impulse at the elbow. Comparisons between measured and predicted parameters reveal the random nature of the slug motion and subsequent impact.



## 1. INTRODUCTION

The Potential damage caused by propelled liquid slugs trapped in voided lines has been a concern in recent years. A number of problems that occurred in nuclear power plants have been reported by Kim (1987) and Merilo *et al.* (1990). For instance, during plant operation, condensate can be formed in the steam lines and trapped at low points of the piping system due to inadequate draining. During start-up or shutdown procedures, or because of abnormal operation of the plant, high-pressure, high-velocity steam enters the lines and entrains the water through the piping, resulting in a two-phase flow. When a threshold velocity is reached, the water fills the entire cross-section of the pipe and becomes a coherent liquid slug. Driven by high-pressure steam, the slug can accelerate rapidly and inflict excessive dynamic loads on tees, elbows or partially open valves. Another mechanism that can create slug motion is water trapped in a loop seal located, for example on the upstream side of a pressurizer saftey-relief valve (Wheeler & Siegel 1982). If under emergency conditions the valve opens very rapidly to relieve excessive pressure, high-pressure steam will accelerate the trapped water into the downstream voided line, thereby possibly creating damage in the pipe and support structures.

When a liquid slug impacts on a pipe discontinuity such as an elbow, a transient hydrodynamic load is imparted to the elbow. This creates an interaction between the liquid and the pipe wall. The level of the damage caused by a slug may vary, depending on characteristics of the system: initial mass and length of the slug, the magnitude of the driving pressure behind the slug, the pipe geometry and the pipe material. An understanding of the

*Presently with the Hydromechanics Laboratory, Department of Civil Engineering, Middle East Technical University, 06531 Ankara, Turkey.

0889–9746/97/080947 + 17 $25.00/fl970112 

hydrodynamics of the slug motion is important in order to mitigate the damage experienced in the piping and pipe supports.

Only two systematic experimental studies investigating the hydrodynamics of individual slug motion have been reported. The first was initiated by Fenton & Griffith (1990), followed shortly thereafter by Bozkus & Wiggert (1991). In the former investigation, the end of the pipe protruded into a copper elbow with some clearance. This elbow was not fastened to the pipe in order to avoid transmission of any vibrations or forces from the pipe to the instrumented elbow section. Subsequent to the impact, the slug was allowed to discharge from the elbow directly into the atmosphere. In the latter study, however, the slug impacted an elbow attached to the pipe and turned 90° to exit a short reach of pipe. It is likely that the character of the slug impact was different in the two experiments. However, both groups of investigators found that even though the pressure peaks at the point of slug impact varied statistically, there was some consistency between experimental peak pressures and those predicted analytically.

The objectives of the present paper are to present the experimental data, describe the analytical model, and compare the results of the present experiments and those of Fenton & Griffith (1990) with numerical predictions.

## 2. EXPERIMENTAL STUDY

Figure 1 shows the general pipe layout used in the experiments. The major components of the experimental apparatus are: an upstream pressure vessel in which air is used as a driving mechanism for slug motion; a 50 mm in diameter, 9·45 m long clear polyvinyl chloride (PVC) pipe containing a fast-acting PVC ball valve; and a 90° elbow located at the downstream end of the pipe reach, followed by a short pipe segment open to the atmosphere. The piping was mounted on seven columns, which in turn were attached rigidly to the concrete floor of the laboratory; in addition, the pipe was rigidly attached to the vessel. As a result of the extensive anchoring, the pipe was considered to be rigid and fully constrained from any significant axial motion induced by the slug impact.

At the elbow, two quartz-crystal pressure transducers were flush-mounted in the pipe wall, one aligned with the longer pipe axis and the other with the shorter pipe axis. The

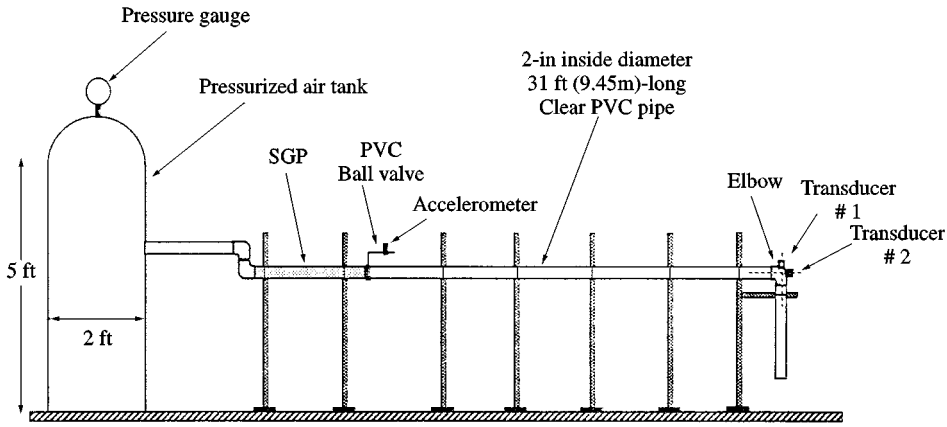


Figure 1. Experimental piping. 1 in = 25·4 mm; 12 in = 1 ft.

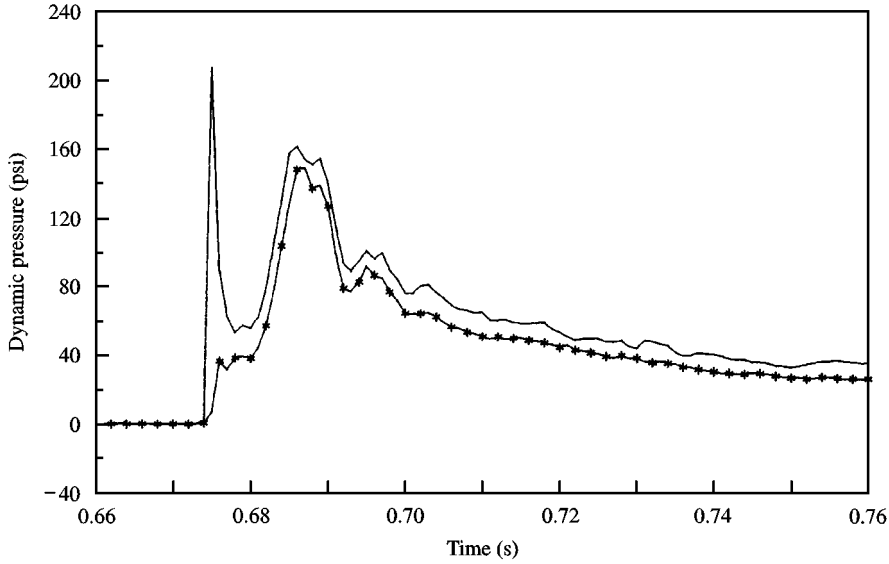


Figure 2. Pressure traces measured at the elbow: $L_i = 11$ ft (3·35 m), $P_0 = 30$ psi (207 kPa): —, Transducer 1; —∗—, Transducer 2, cf. Figure 1.

combined uncertainty in the transient pressure measurements at the elbow was estimated to be $\pm$ 12 kPa for a 500 kPa reading (0 bias, 0·95 probability). A pipe insert labelled SGP for "slug generating pipe" was placed between the tank and the ball valve. It was filled with water prior to opening the valve, thereby providing slugs of the five different initial lengths: $L_i = 1{\cdot}22$, 1·52, 2·13, 2·74 and 3·35 m (4, 5, 7, 9 and 11 ft). A variable-reluctance pressure transducer was used to monitor the pressure in the tank during the transient.

The experiments were performed by first pressurizing the vessel to one of four preset pressures: $P_0 = 70, 138, 207$ and 275 kPa (10, 20, 30 and 40 psi). Then, by rapidly opening the ball valve by hand, a slug of desired length was propelled into the empty pipe. The pressures in the tank and elbow were recorded on a dedicated minicomputer, and the data acquisition was triggered by an accelerometer mounted on the valve handle. Repetitious hand-operated valve motion has been used successfully for traditional fluid transient experiments, and attempts were made to maintain similarly consistent valve motion in the present study. The accelerometer exhibited consistent waveforms for the repeated openings. A rupture disk was not used in place of the ball valve, inasmuch as it was not considered practical because of the costly and time-consuming need to replace it after each experiment.

Pressure traces from the two transducers at the elbow for a representative test are shown in Figure 2. The data subsequently analysed in the study were from the transducer mounted in line with the horizontal pipe axis (Transducer 2), since the more significant impact on the elbow was in that direction. It was observed that peak pressures at the elbow would vary significantly, even though nearly identical initial conditions (i.e. valve opening) were imposed. As a result, each individual test run was repeated 8–10 times, so that average values and standard deviations could be compared with the analytical predictions. Two general trends were observed in the transient pressure measurements. For relatively short slugs ($L_i = 1{\cdot}22$ and 1·52 m), the response exhibited a single peak followed by a rapid depressurization (Figure 3). On the other hand, for relatively long slugs ($L_i = 2{\cdot}13$, 2·74 and 3·35 m) a double-peaked response was observed (Figure 2). Near the elbow, the slugs

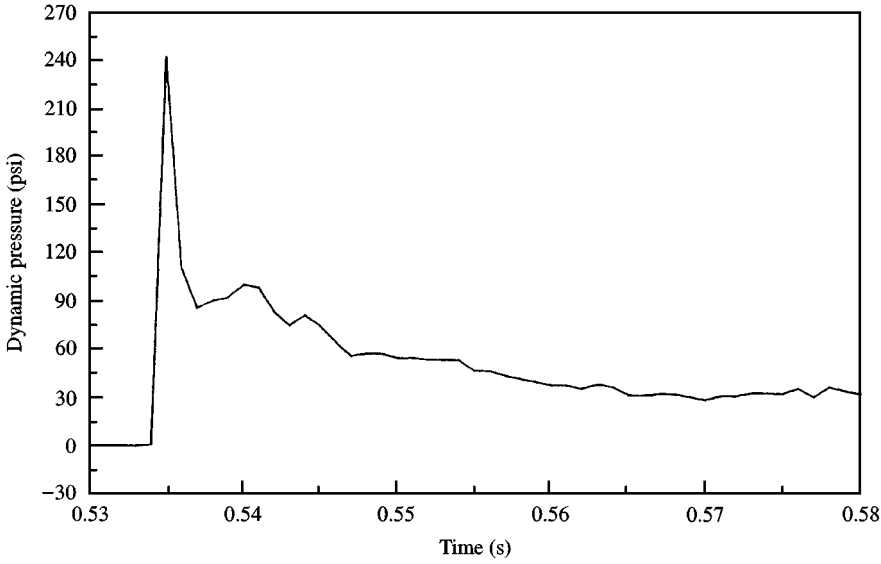


Figure 3. Pressure trace measured at the elbow: $L_i = 5$ ft (1·5 m), $P_0 = 20$ psi (138 kPa).

TABLE 1
Average peak pressures and occurrence time of experimental slugs

| Initial slug length $L_i$ (m) | Initial upstream pressure $P_0$ (kPa) | First pressure peak $P_1$ (kPa) | Second pressure peak $P_2$ (kPa) | First peak time of occurrence $t_1$ (s) | Second peak time of occurrence $t_2$ (s) | Time lag between $P_1$ and $P_2$ $t_1$–$t_2$ (ms) |
|---|---|---|---|---|---|---|
| 3·35 | 69 | 262 | 448 | 1·177 | 1·191 | 14 |
| | 138 | 434 | 855 | 0·834 | 0·845 | 11 |
| | 207 | 717 | 1178 | 0·683 | 0·695 | 12 |
| | 276 | 868 | 1426 | 0·599 | 0·610 | 11 |
| 2·74 | 69 | 386 | 489 | 1·021 | 1·031 | 10 |
| | 138 | 538 | 903 | 0·726 | 0·736 | 10 |
| 2·13 | 69 | 662 | 544 | 0·888 | 0·897 | 9 |
| | 138 | 930 | 1041 | 0·654 | 0·663 | 9 |
| | 207 | 958 | 1530 | 0·546 | 0·557 | 11 |
| | 276 | 1192 | 1819 | 0·475 | 0·484 | 9 |
| 1·52 | 69 | 193 | — | 0·673 | — | — |
| | 138 | 903 | — | 0·524 | — | — |
| 1·22 | 69 | 338 | — | 0·708 | — | — |
| | 138 | 944 | — | 0·539 | — | — |
| | 207 | 979 | — | 0·426 | — | — |
| | 276 | 1495 | — | 0·420 | — | — |

attained speeds as high as 20 m/s. Table 1 shows the average magnitudes of the first and second peak pressures and their arrival times measured at the elbow.

For the longer slug lengths, flow visualization was undertaken to extract some qualitative information regarding the hydrodynamic behaviour of the moving slug. A 400 frame/s

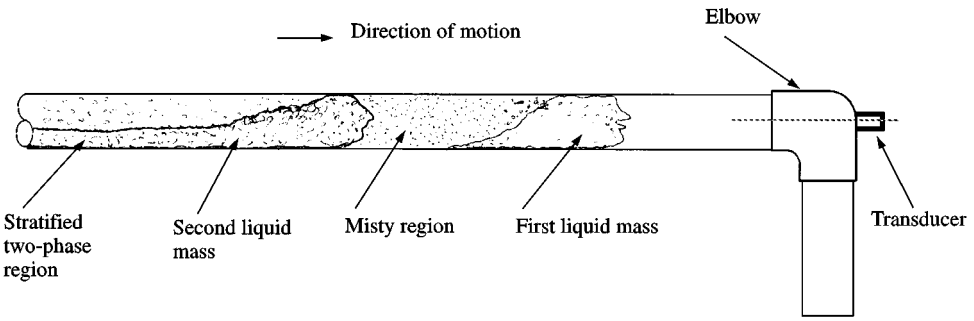


Figure 4. Representation of larger slug flow pattern.

camera with a shutter speed of $\frac{1}{4800}$ s recorded the motion of several slugs just upstream of the elbow; the field of view was approximately 150 mm. It was generally observed that: (i) the leading edge of the slug remained nearly planar; (ii) significant air entrainment had occurred; (iii) the slug ruptured into two distinct masses, the first one a relatively homogeneous air/water mixture separated by a misty region from the second which appeared to be more stratified than the first; and (iv) the trailing edge of the slug consisted of a lengthy stratified two-phase tail with liquid being left behind, a phenomenon called hold-up. Based on these observations a composite sketch of the slug just prior to impact at the elbow was composed (Figure 4). The double-peak phenomenon observed in Figure 2 was correlated with the arrival of the two masses at the elbow. It is uncertain whether the break-up of longer slugs into two masses was due to the action of the upstream valve, the manner in which air entrained at the leading edge of the slug, or both.

## 3. ANALYTICAL AND NUMERICAL DEVELOPMENTS

### 3.1. Slug Motion

The assumptions made to describe the motion of the slug in the voided line are: (i) one-dimensional motion takes place along the pipe axis: (ii) the front face of the slug remains planar; (iii) no air entrainment occurs as the slug accelerates: (iv) shear resistance to slug motion is based on quasi-steady flow; and (v) the slug loses liquid mass at a constant rate due to shearing effects. This mass loss – termed hold-up – is accounted for in the equations with a hold-up coefficient $\alpha$, so that the amount of mass lost per unit length is $\rho(1-\alpha)A$, $0 < \alpha < 1$. The term hold-up refers to the quantity $1-\alpha$.

A moving control volume (Figure 5) is used to formulate the conservation of momentum and mass for the liquid slug accelerating in the voided line. Those relations are

$$\frac{\mathrm{d}U}{\mathrm{d}t} + \left[\frac{f}{2D} - \frac{2}{L}\left(\frac{1}{\alpha} - 1\right)\right] U^2 = \frac{P}{\rho L}, \tag{1}$$

$$\frac{\mathrm{d}L}{\mathrm{d}t} = -\left(\frac{1}{\alpha} - 1\right) U, \tag{2}$$

in which $U$ is the mean slug velocity, $L$ is the slug length, $f$ is the Darcy–Weisbach friction factor, and $P$ is the time-dependent air pressure behind the slug, considered to be an

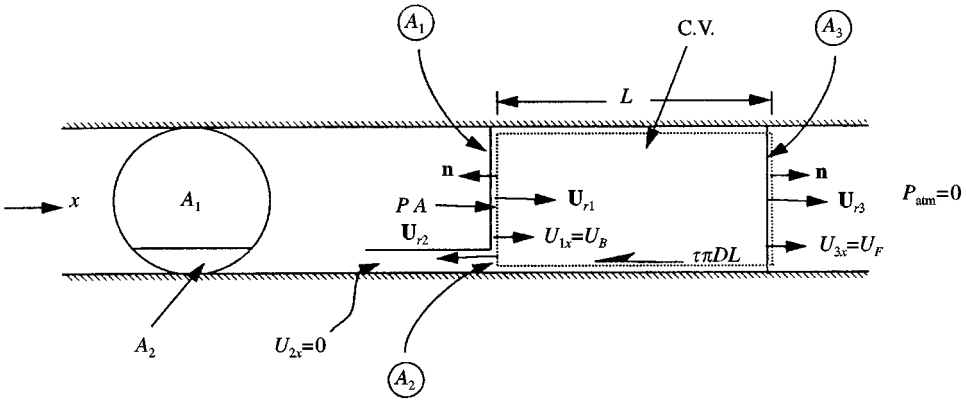


Figure 5. Control volume for moving slug.

unknown. In addition to equations (1) and (2), from the kinematic condition of the moving slug we can write

$$\frac{\mathrm{d}x}{\mathrm{d}t} = U. \tag{3}$$

### 3.2. Gas Dynamics Behind The Moving Slug

In the pipe, the air column present between the upstream tank and the moving slug is treated as one-dimensional, unsteady compressible isothermal flow. The time-variable air pressure in the tank is the known input at the upstream end of the column, and the liquid slug itself becomes the moving downstream boundary. The dynamic equations of the air column are given by Moody (1990) as

$$\frac{\partial P}{\partial t} + V\frac{\partial P}{\partial x} + \rho C^2 \frac{\partial V}{\partial x} = 0, \tag{4}$$

$$\frac{\partial V}{\partial t} + V\frac{\partial V}{\partial x} + \frac{1}{\rho}\frac{\partial P}{\partial x} + \frac{fV|V|}{2D} = 0, \tag{5}$$

$$C = \sqrt{\left(\frac{\partial P}{\partial \rho}\right)_T}. \tag{6}$$

Equations (4)–(6) can be converted to total ordinary differential equations by using the method of characteristics (MOC) procedure. The final equations obtained are as follows.
*Right-travelling characteristic*:

$$\mathrm{d}P + \rho C\,\mathrm{d}V = F\,\mathrm{d}t, \qquad \text{valid on } \frac{\mathrm{d}x}{\mathrm{d}t} = V + C. \tag{7}$$

*Left-travelling characteristic*:

$$\mathrm{d}P - \rho C\,\mathrm{d}V = -F\,\mathrm{d}t, \qquad \text{valid on } \frac{\mathrm{d}x}{\mathrm{d}t} = V - C, \tag{8}$$

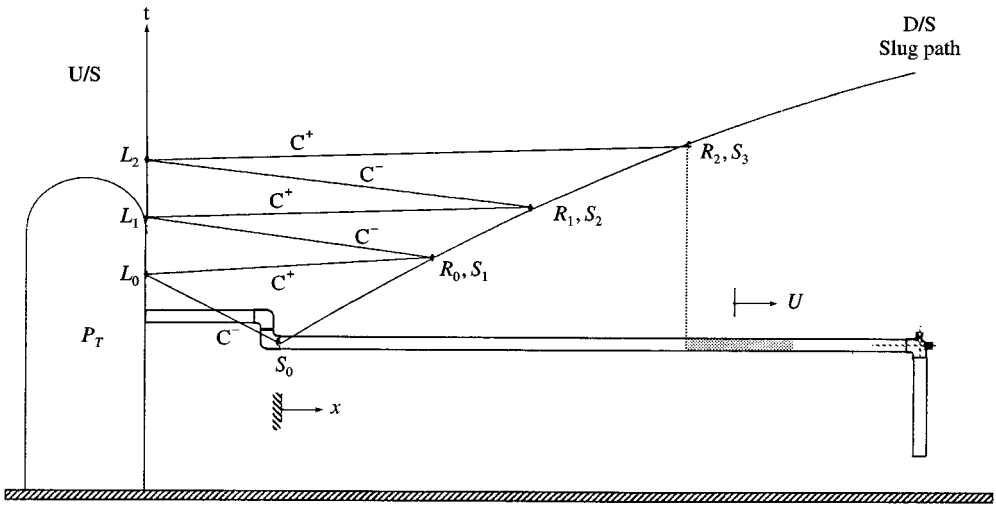


Figure 6. Motion of slug in the $x$–$t$ plane.

where

$$F = -\frac{\rho f C V^2}{2D}. \tag{9}$$

Equations (7) and (8) can be integrated to yield finite-difference equations which can be solved for the unknowns both at the upstream and moving downstream location. Figure 6 shows the characteristic lines and grid system used for the MOC solution. The characteristic lines are constructed such that there are no intermediate nodes; a free-floating grid develops in the $x$–$t$ plane since the intersections of characteristic lines with the boundary nodes are not fixed.

### 3.3. Boundary Conditions

The upstream boundary is located at the pressurized air tank. In the equations, subscript "$a$" denotes air whereas subscript "$w$" denotes water. The following equations are obtained for the upstream boundary:

$$P_L = P_T, \qquad \rho_L = \frac{P_L}{RT}, \tag{10, 11}$$

$$C_L = C = \sqrt{RT}, \quad t_L = t_S + \frac{(x_L - x_S)}{(V - C)_S}, \tag{12, 13}$$

$$\Delta t = t_L - t_S, \tag{14}$$

$$V_L = \frac{P_L - P_S + (\rho_a)_S C V_S}{(\rho_a)_S C \left[ \left( \frac{f_a}{2D} \right) V_S \Delta t + 1 \right]}. \tag{15}$$

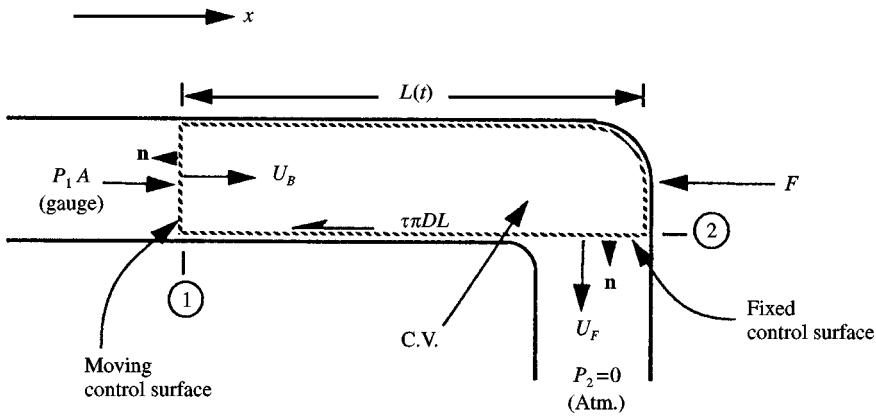


Figure 7. Control volume at the elbow.

The downstream boundary conditions consist of both gas dynamics and slug motion: a right-traveling characteristic in the air column given by equation (7), and equations (1)–(3) for the slug. By integrating equation (7) and combining it with equations (1)–(3), the following solution is obtained:

$$x_R = \frac{U_S(V+C)_L(t_L - t_S) - x_L U_S + x_S(V+C)_L}{(V+C)_L - U_S}, \tag{16}$$

$$\Delta t = \frac{x_R - x_L}{(V+C)_L}, \quad \Delta t_2 = \frac{x_R - x_S}{U_S}, \tag{17,18}$$

$$t_R = t_L + \Delta t_1, \quad L_R = L_S - \left(\frac{1-\alpha}{\alpha}\right) U_S \Delta t_2, \tag{19,20}$$

$$C_R = C = \sqrt{RT}, \quad P_R = P_L + (\rho_a)_L C V_L - \frac{C_1}{C_2}\left[\frac{1}{\rho_w}\left(\frac{P_w - P_{\text{atm}}}{L}\right)_S \Delta t_2 + U_S\right], \tag{21,22}$$

wherein

$$C_1 = \left[f_a \frac{(\rho_a)_L C}{2D} V_L \Delta t_1 + (\rho_a)_L C\right], \tag{23}$$

$$C_2 = \left[1 + \frac{f_w}{2D} U_S \Delta t_2 - 2\left(\frac{1-\alpha}{\alpha}\right)\frac{U_S}{L_S}\Delta t_2\right], \tag{24}$$

$$U_R = \frac{1/\rho_w[(P_w - P_{\text{atm}})/L]_S \Delta t_2 + U_S}{\{1 + (f_w/2D)\, U_S \Delta t_2 - 2\,[(1-\alpha)/\alpha]\;(U_S/L_S)\,\Delta t_2\}}. \tag{25}$$

Note that at the downstream boundary in the air column, the driving pressure is equal to the pressure behind the slug ($P = P_w$) and the velocity is equal to that of the slug ($V = U$). In the equations the pressures are absolute.

### 3.4. Force Generated By Slug Impact At Elbow

Figure 7 shows the control volume applied at the elbow to develop a forcing function that can predict the hydrodynamic loads imparted to the elbow. In addition to the assumptions stated for the moving slug, it is proposed that the slug is destroyed at the elbow, thereby keeping the control surface at section 2 stationary (this assumption is consistent with experimental observations). Applying the conservation of momentum to the control volume of Figure 7 leads to

$$F = P_1 A + \rho A U^2 - \tau \pi D L - \rho L A \frac{\mathrm{d}U}{\mathrm{d}t}, \tag{26}$$

in which $F$ is the resultant force in the $x$-direction acting on the elbow, and $P_1$ is the driving pressure on the back face of the slug. Note that the liquid is assumed to be incompressible, so that no waterhammer-like forces will be predicted. When the shear term is neglected, equation (26) becomes identical to the one employed by Papadakis & Hollingshead (1985). The third and fourth terms on the right-hand side of equation (26) can be shown to be negligible relative to the first and second terms, so that the relation is reduced to the form employed to predict the load on the elbow, i.e.

$$F = P_1 A + \rho A U^2. \tag{27}$$

The equations that govern the slug dynamics were normalized (Bozkus 1991) using the following parameters: $P_0$, $U_0 = \sqrt{P_0/\rho}$, $L_0 = 2D(2 - 1/\alpha)/f$ and $t_0 = L_0/U_0$. The above scale factors were used to scale the dimensional variables slug velocity $U$, slug length $L$, slug

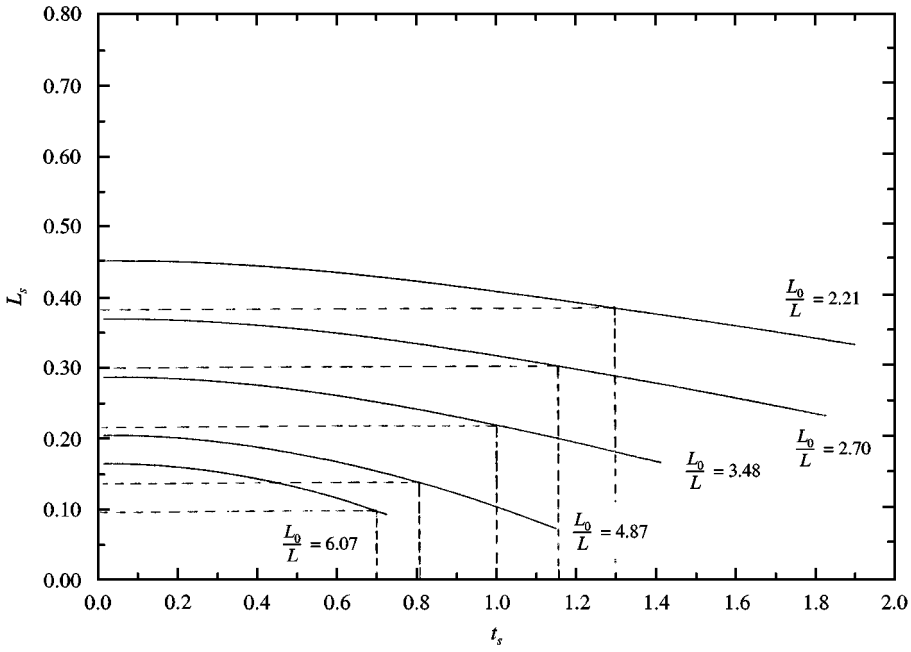


Figure 8. Scaled slug length versus scaled time.

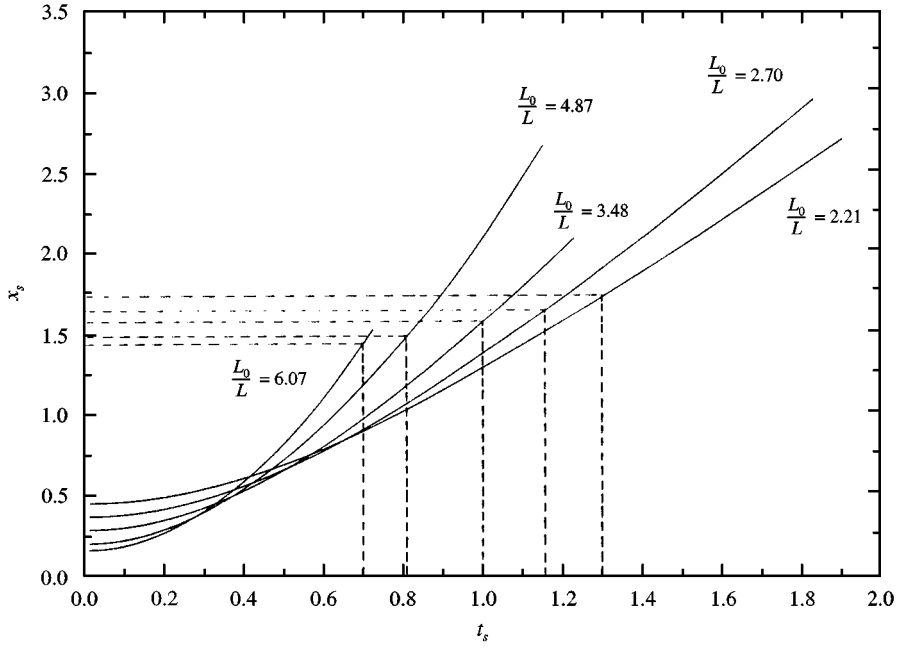


Figure 9. Scaled slug position versus scaled time.

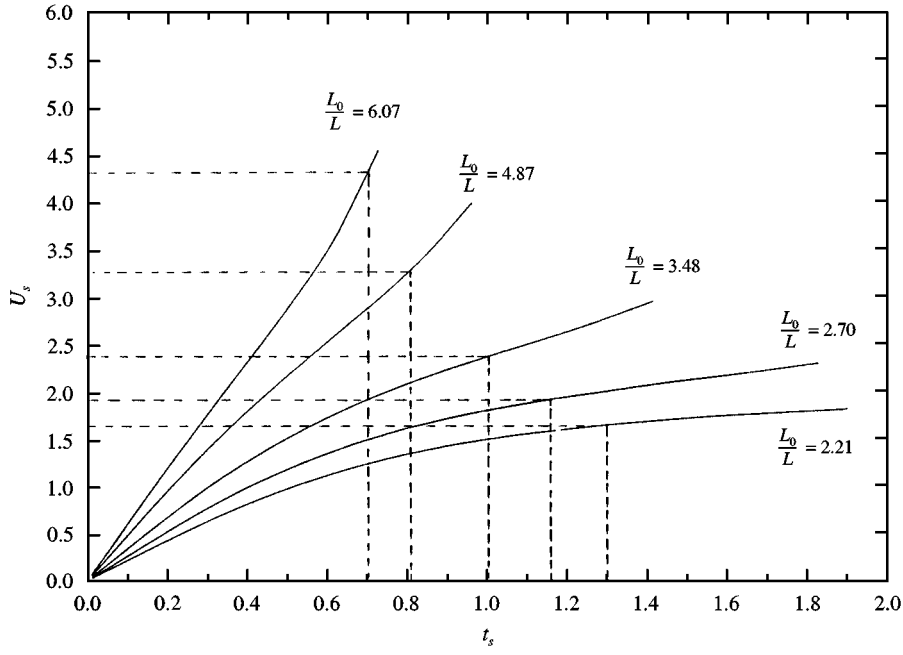


Figure 10. Scaled slug velocity versus scaled time.

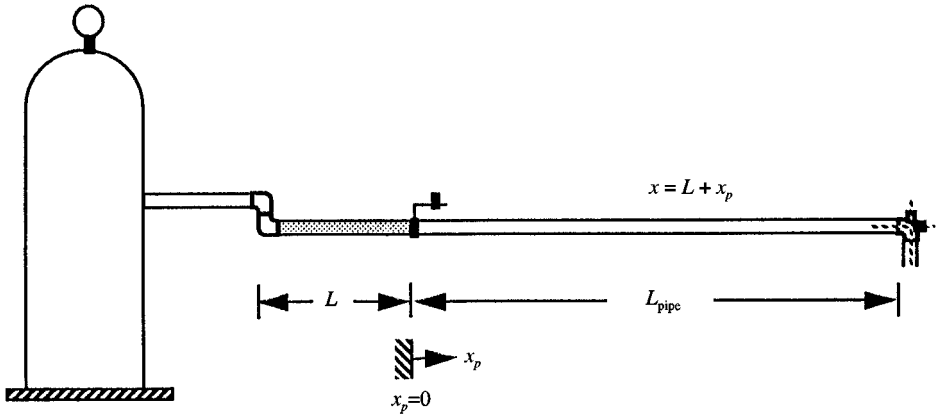


Figure 11. Coordinate system used for the slug position.

position $x$ and time $t$. In Figure 8–10 are shown the numerical results in scaled form for all of the experimental test conditions. Figure 8 shows slug length versus time, Figure 9 shows slug position versus time and Figure 10 exhibits the time history of the slug velocity. Each of the five curves in the figures is drawn for a fixed ratio of the length-scale factor to the initial slug length, $L_0/L_i$. The vertical line drawn for each curve signifies the instant at which the slug arrives at the elbow. The horizontal lines in Figures 8–10 designate the length, position and velocity of the slug at the instant it reaches the elbow. Note that the slugs do not start at the same position, because of the coordinate system chosen for the position of the slug (Figure 11).

A hold-up coefficient $\alpha = 0{\cdot}95$, that is 5% hold-up based on observed data, was employed. As $\alpha$ is decreased, the velocity of a slug will increase and its length will decrease as it accelerates towards the elbow. A constant friction factor $f = 0{\cdot}013$ was calculated based on quasi-steady flow in a smooth pipe. Figure 8 indicates that short slugs (i.e. $L_0/L_i = 6{\cdot}07$) lose more of their initial length and mass than long slugs by the time they reach the elbow. This is apparent in the slopes of the curves in Figure 8. As the initial slug length increases, the slope of the curves become milder, indicating a slower rate of decrease in the slug length for the long slugs. It is seen in Figure 10 that short slugs accelerate much more quickly than long slugs, due to their initial smaller masses and higher mass loss rate during their motion in the pipe. For instance, the 1·22 m (i.e., 4 ft) long slug impacts at the elbow with a velocity that is about three times greater than that of the 3·35 m (i.e. 11 ft) long slug. Figures 8–10 can be used independently in similar pipe systems to estimate variables such as velocity, arrival time, and length and position of the slug.

## 4. COMPARISON OF NUMERICAL MODEL WITH EXPERIMENTAL DATA

### 4.1. Peak Pressures At The Elbow

Figure 12 shows the peak pressures for the experiments and the numerical predictions versus the distance that the slug travelled. The initial reservoir pressure $P_0$ was used to normalize the peak pressures. Each vertical line represents one set of experiments for a particular initial slug length $L_i$. The solid circle indicates the mean value, the intermediate dashes the standard deviation, and the top and bottom dashes the extreme values obtained

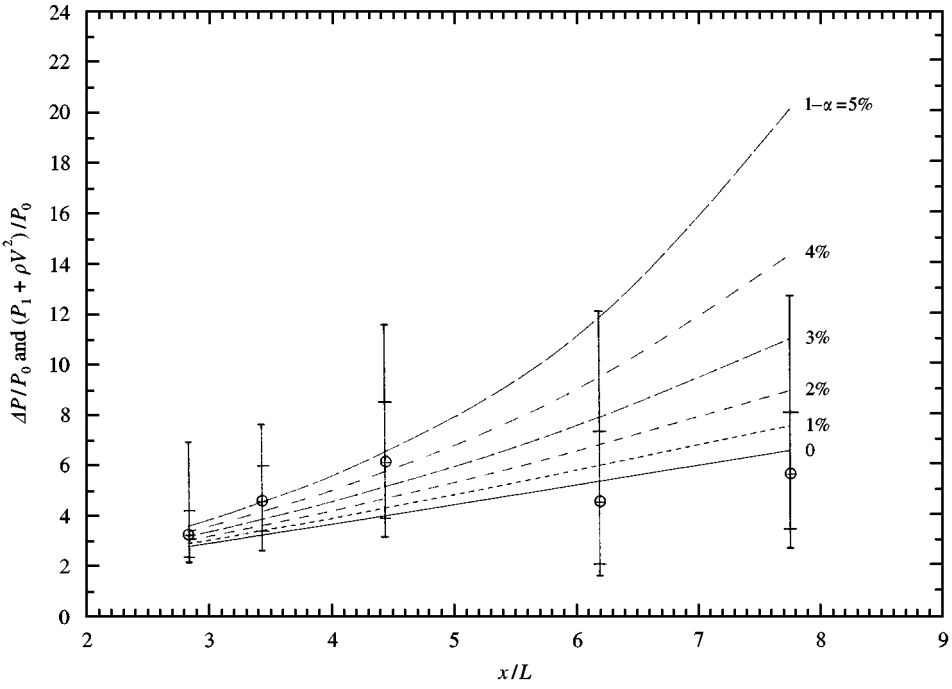


Figure 12. Experimental and predicted normalized pressure peaks at the elbow versus relative travel length for various values of holdup, $\alpha$; $f = 0{\cdot}013$.

in that particular set of experiments. For the longer slugs, where the double-peak phenomenon was observed, the first peak value was chosen as the experiment $\Delta P$. The numerical simulations are presented in Figure 12 as six curves, each associated with a different hold-up coefficient ranging from 0 to 5%. The parameter plotted on the ordinate scale is the normalized predicted pressure rise at the elbow, assuming that the resultant force at the elbow in the $x$-direction is dominated by the driving pressure $P_1$ immediately upstream of the elbow and the complete break-up of the $x$-component of momentum flux $\rho U^2$.

A reasonable agreement between the mean values of the recorded and simulated peaks is apparent for the longer slug lengths ($x/L < 5$) when the hold-up rates vary from 3 to 5%. For shorter slugs ($x/L > 5$), the mean experimental values fall below the predictions, even with zero hold-up; in part this may be attributed to the observation that the short slugs were subjected to significant air entrainment, which would tend to reduce the mean density of the slug, and consequently lower the peak dynamic pressures.

### 4.2. Normalized Forces At The Elbow

The normalized peak force at the elbow is defined as

$$F^* = \frac{\Delta P}{P_1 + \rho U^2} \tag{28}$$

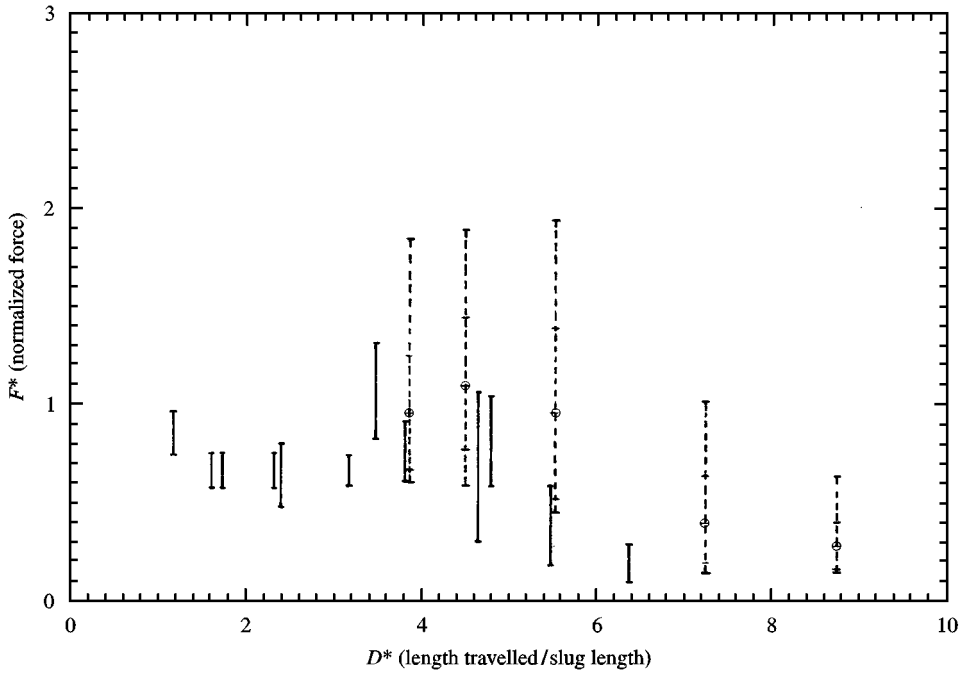


Figure 13. Normal force versus dispersion distance: ———, Fenton & Griffith (1990); – – –, present study.

and is plotted in Figure 13 versus the so-called dispersion distance $D^* = x/L_i + 1$ (Fenton & Griffith 1990). Two groups of experimental data spread are shown: the solid lines are the data of Fenton & Griffith (1990) with $P_1 = 0$ and no hold-up, and the dashed lines are the present study with $P_1 \neq 0$ and 5% hold-up. The reason Fenton & Griffith set $P_1 = 0$ is because the slug exited the pipe immediately after impacting the elbow. They argued that the pressure difference between a point in liquid slug in the vicinity of the elbow and the exit of the elbow was not significant. In the present study, $P_1$ could not be neglected since the elbow was attached to a short pipe segment through which the slug exited into the atmosphere.

The parameter $F^*$ would be unity if the measured and predicted forces were in complete agreement. As seen in Figure 13, there is more data scatter for the present study than that of Fenton & Griffith. In comparison, the present study had a pipe diameter that was twice as large, the pipe was horizontal as opposed to being slightly inclined in the direction of slug motion, and initially the slug was forced to travel through a ball valve instead of a ruptured disk. Those situations may have given rise to greater variation in the slug motion and subsequent impact. In spite of the differences in spread of the data, there are observable trends in the mean values to which both studies conform. The normalized force $F^*$ remains slightly below unity for $D^* < 3$, rises above unity for $3 < D^* < 5$ and then rapidly drops below unity for $D^* > 5$. The reason for the pronounced drop in $F^*$ for $D^* > 5$ is likely due to air entrainment and rapid deterioration of the relatively short slugs. The shortest slugs in the experiments ($D^* \simeq 8{\cdot}8$) were those which nearly lost all of their mass due to hold-up before they reached the elbow. The force prediction of Fenton & Griffith appears to be overestimated in the region of $D^* < 5$, and at greater dispersion rates ($D^* > 5$) the overestimation is higher. Although the data scatter from the present study is greater, the mean

values of the normalized forces of the present study (shown as circles on the dashed lines) fall closely around unity in the region $D^* < 6$ where relatively longer slugs are present.

### 4.3. Normalized Impulse Loads At The Elbow

The experimental impulse at the elbow is defined as the integral of the pressure–time history multiplied by the pipe cross-sectional area:

$$I_{\text{rec}} = A \int p(t)\, \mathrm{d}t, \tag{29}$$

in which $p(t)$ is the dynamic pressure measured in the $x$-direction at the elbow. The integral limits were based on the observations that the most significant pulses occurred within the first 100 ms of the transient; the lower limit represents the instant at which the slug arrived at the elbow, and the upper one is the instant when the measured magnitude of the impact pressure at the elbow dropped below the initial upstream reservoir pressure. It was observed that between these limits, the most significant portion of the waveform had passed.

In order to normalize the experimental impulse $I_{\text{rec}}$, an analytical impulse, $I_m$, was defined as the area under the predicted pressure–time history. The normalized impulse is then given by

$$I^* = \frac{I_{\text{rec}}}{I_m}. \tag{30}$$

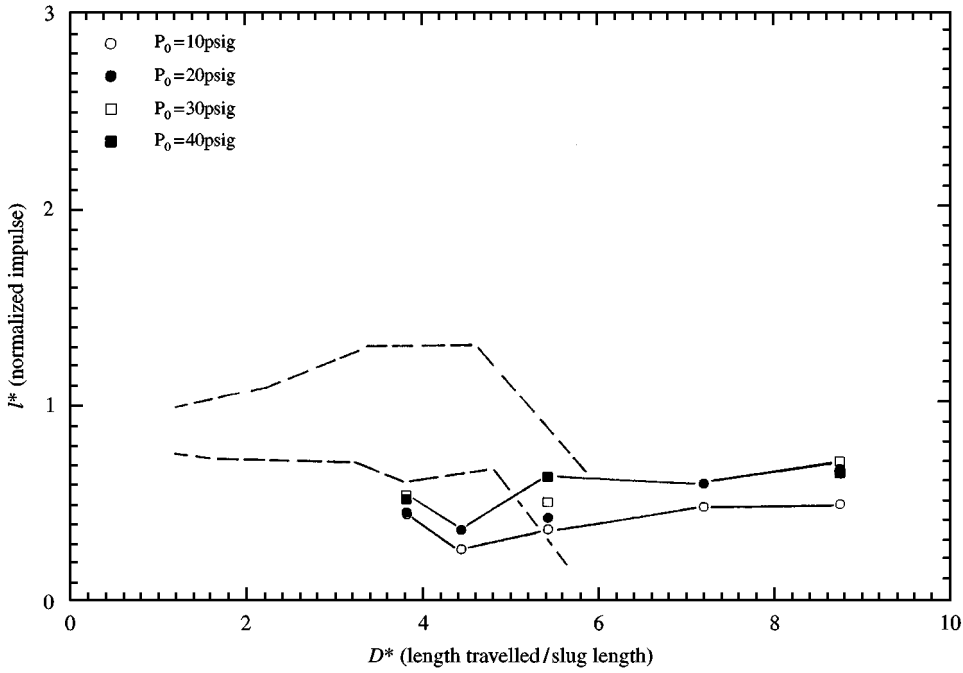


Figure 14. Spread of normalized impulse versus dispersion distance: – – –, Fenton & Griffith (1990); ———, present study; 10 psi = 68·97 kPa.

Figure 14 shows the spread of the normalized impulses measured at the elbow for both the Fenton & Griffith and the present study. The discrepancies between the two studies may be based in part on the manner in which the respective integral limits are defined in equation (29). As a result, the present study tends to overpredict the impulses at the elbow. In addition, the same mechanisms that reduce the measured forces, as mentioned above, may contribute to lower normalized impulses for values of $D^* > 5$.

### 4.4. Significance Of Slug Motion To Piping Response

The impact of a moving slug on a piping system can create significant forces (Wheeler & Siegel 1982), resulting in either substantial pipe motion or yielding of piping and pipe supports. In the present study, the pipe was rigidly anchored and restrained from any significant motion. Any movement that would have resulted from the slug impacting the elbow would have been a high-frequency, small-amplitude axial vibration, which would not have interacted with the hydrodynamic impulsive loading to any appreciable degree. The results presented herein can provide a methodology for estimating the response induced by a liquid slug impacting a piping system. Using Figure 13, the peak pressure can be scaled, and a representative waveform can be formulated. For example, a triangular- or square-wave-shaped pressure pulse with a known duration (the residence time of the slug through the discontinuity) will constitute the waveform. The resulting impact of the slug is of such short duration that the impulsive load can be input as an external forcing function to a piping dynamic analysis. What is necessary to acquire is additional data related to slug motion in prototype piping systems, so that the effects of higher velocities, larger driving pressures, air entrainment and the larger dimensions can be ascertained.

## 5. DISCUSSION AND CONCLUSIONS

The experimental phase of the present study clearly demonstrates the complex behaviour of slug flow. Flow visualization indicated that almost all of the slugs were subjected to significant air entrainment as they accelerated into the voided pipe. Moreover, the larger slugs were observed to break up into two distinct masses. Despite nearly identical initial conditions (slug length, upstream air-tank pressure), and even though the pressure traces are similar for a given slug length, arrival times and peak pressures recorded at the elbow exhibited some variation. This can be partly attributed to the nature of the valve opening, although it was considered to be fairly repeatable, but not completely so. For the shorter slugs that travelled greater than six times their length prior to impact, the measured forces at the elbow dropped significantly. That phenomenon is suspected to be caused by air entrainment, slug erosion and penetration of the driving gas bubble, i.e. hold-up.

The results of the series of experiments carried out for liquid slugs of various lengths driven by pressurized air were used to verify a mathematical model that accounts for loss of liquid mass of the accelerating slug as well as transient flow of the driving gas in the pipe behind the accelerating slug. Once the slug reaches the elbow, incompressible momentum-transfer theory is utilized to predict the impulse at the elbow. The impact forces at the elbow are caused primarily by destruction of the horizontal component of momentum of the slug. The mathematical model does not account for the air entrainment in the slug dynamics, hence the predictions for the peak impact pressure $\Delta P$ are on the

conservative side, especially for the short slugs which are most prone to air entrainment. Hold-up is shown to have an effect on the predicted pressure peaks at the elbow, and a suggested upper bound for hold-up is 5%. Normalized forces (Figure 13) of the present study show trends similar to those presented by Fenton & Griffith (1990), but with a larger variation.

A number of mechanisms affecting the resultant forces or pressure peaks due to slug motion can be present in large-scale industrial piping that are not accounted for in the present study. Two such mechanisms are steam-bubble collapse and waterhammer-induced forces. However, the effects of air entrainment and hold-up on the resulting impact forces are clearly demonstrated. Inherent in such flows is the element of uncertainty when attempting to predict the slug dynamics. Yang & Wiggert (1998) developed a quasi-two-dimensional two-phase flow cylindrical model of the slug motion and postulated that an acoustic, waterhammer-like response may occur at the elbow for the shorter slugs in the present study, but not in a consistent manner. That uncertainty demonstrates the need to obtain experimental data of slug motion in large piping with higher driving pressures, and to ascertain the suitability of one-dimensional models on such systems.

## ACKNOWLEDGEMENTS

Appreciation is extended to Michigan State University for providing an All-University Research Initiation Grant for a portion of the study.

## References

Bozkus, Z. 1991 The hydrodynamics of an individual transient slug in a voided line. Ph.D. dissertation, Department of Civil and Environmental Engineering, Michigan State University, East Lansing, MI, U.S.A.

Bozkus, Z. & Wiggert, D. C. 1991 Slug motion and impact in a voided line. In *Fluid Transients and Fluid Structure Interaction* (eds D.C. Wiggert & F. J. Moody), PVP-Vol. 224/FED-Vol. 126, pp. 25–27. New York: ASME.

Bozkus, Z. & Wiggert, D. C. 1992 Hydromechanics of slug motion in a voided line. In *Unsteady Flow and Fluid Transients* (eds. R. Bettess & J. Watts), pp. 77–86. Rotterdam: A.A. Balkema.

Fenton, R. M. & Griffith, P. 1990 The force at a pipe bend due to the clearing of water trapped upstream. In *Transient Thermal Hydraulics and Resulting Loads on Vessel and Piping Systems*, (eds. F. J. Moody, Y. W. Shin & J. Colton) PVP-Vol. 190, pp. 59–67. New York: ASME.

Kim, J. H. 1987 Water hammer prevention, mitigation and accommodations: a perspective. *Transactions of the American Nuclear Society* **55**, 733–734.

Merilo, M., Van Duyne, D. A., Safwat, H. H. & Arastu, A. H. 1990 Reducing the frequency of water hammer in nuclear power plants. In *Transient Thermal Hydraulics and Resulting Loads on Vessel and Piping Systems* (eds. F. J. Moody, Y. W. Shin & J. Colton), PVP-Vol. 190, pp. 1–7. New York: ASME.

Moody, F. J. 1990 *Introduction to Unsteady Thermofluid Mechanics*, New York: Wiley.

Papadakis, C. N. & Hollingshead, D. 1985 Transients in empty pipes subject to rapid filling. In *Proceedings Hydraulics Division Specialty Conference on Hydraulics and Hydrology in the Small Computer Age*. pp. 1376–1381, New York: ASCE.

Wheeler, A. J. & Siegel, E. A. 1982 Measurements of forces in a safety valve discharge line. ASME Paper 82-WA/NE-8, New York: ASME.

Yang, Jiandong & Wiggert, D. C. 1998 Analysis of liquid slug motion in a voided line. *ASME Journal of Pressure Vessel Technology* **120** (in press).

## APPENDIX: NOTATION

| | |
|---|---|
| $A$ | pipe cross-sectional area |
| $C$ | wave speed in air column |

| | |
|---|---|
| $D$ | internal pipe diameter |
| $D^*$ | dispersion distance |
| $f$ | Darcy–Weisbach friction factor |
| $F$ | instantaneous force at elbow |
| $F^*$ | normalized peak force |
| $I_{\text{rec}}$ | recorded impulse at the elbow |
| $I_m$ | derived impulse |
| $L_i$ | initial slug length |
| $L$ | instantaneous slug length |
| $L_0$ | scaling factor for length |
| $P$ | instantaneous pressure in air column |
| $P_0$ | initial reservoir pressure, and scaling factor for pressure |
| $P_1$ | predicted pressure at elbow |
| $R$ | gas constant |
| $T$ | absolute temperature |
| $t$ | time |
| $t_0$ | scaling factor for time |
| $U$ | mean slug velocity |
| $U_0$ | scaling factor for velocity |
| $V$ | velocity in air column |
| $x$ | slug position |
| $\alpha$ | holdup coefficient |
| $\rho$ | density |
| $\tau$ | fluid wall shear stress |
| $\Delta P$ | recorded peak pressure due to slug impact |

*Subscripts*

| | |
|---|---|
| $a$ | air |
| $L, R, S$ | locations on the time-space grid |
| 0 | scale factors |
| $s$ | scaled (dimensionless) variables |
| $T$ | tank |
| $x$ | pipe axial direction |
| $w$ | water |